Received: 31 December 2017 | Accepted: 18 May 2018

DOI: 10.1002/jcb.27147

RESEARCH ARTICLE

WILEY Journal of Cellular Biochemistry

Benzimidazoles as novel deoxyribonuclease I inhibitors

Ana Kolarević[1] | Budimir S. Ilić[2] | Neda Anastassova[3] | Anelia Ts. Mavrova[4] | Denitsa Yancheva[3] | Gordana Kocić[5] | Andrija Šmelcerović[2]

[1]Department of Pharmacy, Faculty of Medicine, University of Niš, Niš, Serbia

[2]Department of Chemistry, Faculty of Medicine, University of Niš, Niš, Serbia

[3]Laboratory of Structural Organic Analysis, Institute of Organic Chemistry with Centre of Phytochemistry, Bulgarian Academy of Sciences, Sofia, Bulgaria

[4]Department of Organic Synthesis, University of Chemical Technology and Metallurgy, Sofia, Bulgaria

[5]Department of Biochemistry, Faculty of Medicine, University of Niš, Niš, Serbia

Correspondance
Andrija Šmelcerović, Department of Chemistry, Faculty of Medicine, University of Niš, Bulevar Dr Zorana Đinđića 81, 18000 Niš, Serbia.
Email: a.smelcerovic@yahoo.com; andrija.smelcerovic@medfak.ni.ac.rs

Funding information
Ministry of Education, Science and Technological Development of the Republic of Serbia, Grant/Award Numbers: OI 171025, OI 172044, TR 31060; Faculty of Medicine of the University of Nis, Grant/Award Number: Internal project No. 4

Abstract

Inhibitory potential of 19 benzimidazoles against bovine pancreatic deoxyribonuclease I (DNase I) was investigated in vitro. Three compounds inhibited DNase I with IC_{50} below 100 μM and proved to be more potent DNase I inhibitors than crystal violet ($IC_{50} = 351.82 \pm 29.41$ μM), used as a positive control. Compound **9** showed the most potent DNase I inhibition with an IC_{50} value of 79.46 ± 11.75 μM. To further explore the relationship between inhibitory activity and 2D pharmacophore features, Pharma/E-State R-group quantitative structure-activity relationship (RQSAR) models were generated and validated using Schrödinger Suite. RQSAR models showed a significant enhancement of benzimidazoles activity using hydrogen-bond acceptor substituents at the R2, R3, and R4 positions, or aryl substituents at the R4 position. The Site Finder module and molecular docking defined the benzimidazoles interactions with the most important catalytic residues of DNase I, including H-acceptor interaction with residue His 134 and His 252 and/or H-donor interaction with residue Glu 39. We also found a positive correlation between IC_{50} inhibition values and relative binding free energies of the most active benzimidazoles. In addition, a molecular dynamics simulation was performed for DNase I-compound **9** docking complex in Desmond. Trajectory analysis showed that docking complex and intermolecular interactions were stable throughout the entire production part of simulations. Furthermore, the results of protein structure alignment module suggested the potential translational impact of benzimidazoles against human DNase I. Due to the significant involvement of DNase I in the pathophysiology of many disease conditions, benzimidazoles as DNase I inhibitors could have potential therapeutic applications.

KEYWORDS

benzimidazoles, deoxyribonuclease I (DNase I) inhibition, molecular docking, molecular dynamics simulations, pharmacophore modeling, R-group analysis

1 | INTRODUCTION

An inappropriate balance between cell proliferation and cell death results in either cell accumulation or cell loss, consequently contributing to the pathogenesis of various human diseases. Increased apoptosis can result from acquired or genetic conditions that enhance the accumulation of signals that induce apoptosis or decrease the threshold at which such conditions induce apoptosis.[1] Excessive cell death has been observed among patients with autoimmune disorders (AIDS),[2] neurodegenerative disorders (Alzheimer's disease, Parkinson's disease,

Huntington's disease, amyotrophic lateral sclerosis, retinitis pigmentosa, spinal muscular atrophy, cerebellar degeneration),[1-4] graft-versus-host disease,[5] ischemic injuries (myocardial infarctions and stroke),[1,6,7] and acute fatty degeneration of the liver (induced by various toxins, including alcohol).[8] Deoxyribonuclease I (DNase I), a Ca^{2+}/Mg^{2+}-dependent endonuclease, is considered one of the main nucleases involved in DNA fragmentation during apoptosis,[5,9-13] and thus might be involved in the pathophysiology of such diseases. Elevated DNase I levels, together with increased DNA fragmentation, have been determined in conditions such as idiopathic dilated cardiomyopathy,[14] type 2 diabetes,[15,16] cisplatin-induced nephrotoxicity,[17-19] acetaminophen-induced hepatocellular necrosis,[20] and gamma radiation-induced injuries in several radiosensitive organs (intestine, bone marrow and white pulp of the spleen).[21] These data indicate the potential application of DNase I inhibitors in the treatment of such diseases. However, the number of known organic DNase I inhibitors, either natural or synthetic, is relatively small,[22] including 2-nitro-5-thiocyanobenzoic acid,[23] 2-nitro-5-thiosulfobenzoic acid,[24] nitrogen mustard,[25] and crystal violet.[26] Therefore, discovery of novel organic DNase I inhibitors, especially those with potential therapeutic applications, represents an attractive research field.

Benzimidazole derivatives exhibit numerous pharmacological activities, including analgesic, anthelmintic, antiallergic, anticancer, anticoagulant, antidiabetic, anti-HIV, antihypertensive, anti-inflammatory, antimicrobial, antimycobacterial, antioxidant, antiparasitic, antiulcer, antiviral, anxiolytic, central nervous system stimulant, coagulant, depressant, and also act as hormone modulators, immunomodulators, lipid level modulators, and proton pump inhibitors.[27-29] Some of them have been clinically approved, such as albendazole, mebendazole, and thiabendazole as anthelmintics; lansoprazole, omeprazole, and pantoprazole as proton pump inhibitors; astemizole as antihistaminic; enviradine as antiviral; and candesartan and telmisartan as antihypertensive agents.[30] Benzimidazole heterocycle is a structural isostere of the purine base, which is a component of the nucleotides. To find novel organic DNase I inhibitors, continuing our research on the synthesis and pharmacological activities of benzimidazoles,[31-35] in the current study, 19 benzimidazoles, including five 1,3-disubstituted-benzimidazole-2-imines (group A, **1**-**5**) and four 2-substituted-1,3-thiazolo[3,2-*a*]benzimidazolones (group B, **6**-**9**) synthesized by Mavrova et al[36] as well as ten 1,3-disubstituted-benzimidazole-2-thiones (group C, **10**-**19**) synthesized by Anastassova et al[37] were evaluated for inhibitory activity against bovine pancreatic DNase I in vitro (Table 1). R-group analysis, 3D pharmacophore modeling, molecular docking, molecular dynamics simulations, and protein structure alignment are in silico drug design methods used for better understanding drug properties and target interaction that hypothesize the designing of novel drug candidates.[38] Keeping in mind that our studied molecules were built on a similar scaffold, by attaching different groups at one or more points on the benzimidazole ring, we wanted to examine the DNase I inhibitory property of the benzimidazoles as a function of the groups at the various attachment points. As a result of missing X-Ray diffraction/nuclear magnetic resonance atomic-level details between small organic inhibitor and bovine pancreatic DNase I,[39] 3D pharmacophore modeling were used. We hoped that feature geometries common to the active benzimidazoles will contain information related to the important interactions between the bound conformations of the active benzimidazoles and DNase I. In addition, we wanted to clarify the DNase I inhibitory properties of benzimidazoles at the molecular level using the Site Finder module, molecular docking studies, molecular dynamics simulations, and protein structure alignment.

2 | MATERIALS AND METHODS

2.1 | Synthesis

The synthesis of the studied compounds, five 1,3-disubstituted-benzimidazole-2-imines (**1**-**5**), four 2-substituted-1,3-thiazolo[3,2-*a*]benzimidazolones (**6**-**9**) and ten 1,3-disubstituted-benzimidazole-2-thiones (**10**-**19**), was described in our previous publications.[36,37]

2.2 | Evaluation of DNase I inhibition

DNase I from bovine pancreas, DNA, dimethyl sulfoxide (DMSO) and perchloric acid were purchased from Sigma-Aldrich (St. Louis, MO). Crystal violet was purchased from Lach-Ner (Neratovice, Czech Republic).

DNase I from bovine pancreas was used for in vitro evaluation of enzyme inhibition by spectrophotometric measurement of acid-soluble nucleotides formation at 260 nm (method slightly modified by Bartholeyns et al[40]). The inhibition was studied in a series of test-tubes with the reaction mixture (total volume 1040 μL), prepared in the following order: (a) test samples contained 80 Kunitz units of DNase I, one of the studied compounds (**1**-**19**) diluted in DMSO (the final concentration of DMSO in the assay was 3.85% v/v), 0.0077% of DNA, and 80.77 mM Tris-HCl buffer (pH 7.6); (b) solvent control samples contained the same amount of DNase I, appropriate amount of DMSO, DNA and Tris-HCl buffer. Corresponding blank samples were prepared for each group in the same way as the test solutions (a and b).

TABLE 1 Chemical structures of benzimidazoles **1-19**

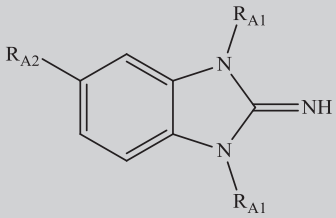

Group A (1-5)

Compound	R_{A1}	R_{A2}
1	CH_2CO_2Et	COPh
2	CH_2CO_2Et	Me
3	$(CH_2)_3Ph$	Me
4	CH_2COPh	Me
5	CH_2COPh	NO_2

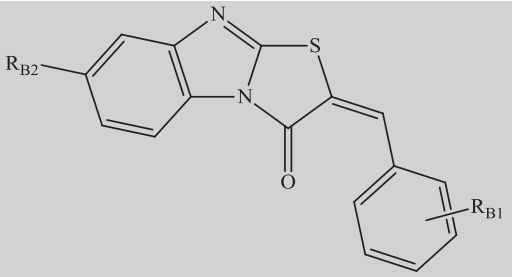

Group B (6-9)

Compound	R_{B1}	R_{B2}
6	*o*-Me	COPh
7	*o*-F	COPh
8	*p*-F	COPh
9	1,3-Dioxolyl	COPh

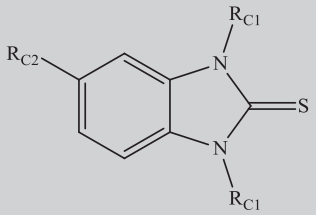

Group C (10-19)

Compound	R_{C1}	R_{C2}
10	$(CH_2)_2CO_2Me$	H
11	$(CH_2)_2CO_2Me$	Me
12	$(CH_2)_2CO_2Me$	NO_2
13	$(CH_2)_2CO_2Me$	Cl
14	$(CH_2)_2CO_2Me$	COPh
15	$(CH_2)_2CONHNH_2$	H
16	$(CH_2)_2CONHNH_2$	Me
17	$(CH_2)_2CONHNH_2$	NO_2
18	$(CH_2)_2CONHNH_2$	Cl
19	$(CH_2)_2CONHNH_2$	COPh

After incubation at 37°C for 30 minutes the reaction was stopped by adding 80 μL of perchloric acid. The percentage of enzyme inhibition was determined by measuring the difference in absorbance that correlates with acid-soluble nucleotides formation; it was calculated as a percentage of specimen absorbance versus absorbance of the solvent control samples. All samples containing one of the studied compounds (**1**-**19**) were assayed for DNase I inhibitory activity at a concentration of 200 μM. Those showing inhibition greater than 50% at these concentrations were tested in a broader concentration range to allow calculation of IC_{50} values. IC_{50} curves were generated using 4 concentrations of the studied compounds (200, 150, 100, and 50 μM). Crystal violet was used as positive control. All experiments were performed in triplicate and averaged.

2.3 | In silico studies

R-group analysis

Pharma/E-State RQSAR models Pharma/E-State RQSAR models analyzed the benzimidazoles activity as a function of the kind of R-group at each attachment position, and displayed the results qualitatively in terms of increasing, decreasing, or having a little effect on the activity.[38] We ran a partial-least-squares procedure that fitted the observed inhibitory data to the counts of the features present in each R-group at each position. For Pharma/E-State RQSAR models, the counted features are the pharmacophore types and various E-state atom types.[38] This was done using a 75%: 25% random training: test-set split. The procedure was repeated 100 times, picking each time the model that does the best job without overfitting. For each model, each pharmacophore/E-state feature type at each R-group position was given a coefficient that reflects how much it contributes to the property being modeled. A feature type was deemed significant (colored red or blue) if the absolute value of the mean of its coefficients over the models exceeded the importance cutoff, which is a statistic, computed from all coefficients over all models.

Importance analysis Importance analysis addressed the question of how sensitive the DNase I inhibitory property of the studied benzimidazoles was to R-group variation at a specific position. A position was more important than the other, if the variation of the R-group at that position led to greater property differences than those observed when the R-group varied at the other position. The importance value of a position was the range of the property over the R-groups at a specific position averaged over all structures containing a given R-group at that position.

3D Pharmacophore modeling

Pharmacophore mapping was carried out using PHASE version 4.2 available in Maestro 10.1 molecular modeling package from Schrödinger.[41] Pharmacophore modeling is the qualitative picture for finding the chemical feature for the active site geometry and spatial arrangements in 3D space of the ligands. There are 6 in-built pharmacophore features available in PHASE: hydrogen bond acceptor (A), hydrogen bond donor (D), hydrophobic group (H), negative charged group (N), positive charged group (P) and aromatic ring (R). Common pharmacophore features were used to construct pharmacophore sites. For defining a pharm-set in PHASE, an activity threshold range was selected in such a way that compounds were active if IC_{50} value was below 200 μM and inactive if IC_{50} value was above 200 μM. The common pharmacophore hypotheses were generated with default settings. A pharmacophore cluster was proceeded based on the highest average similarity. The preferred hypothesis was then selected based on the survival score.

Molecular docking

Ligand preparation Examined benzimidazoles were built with ChemBioDraw Ultra 13.0 (PerkinElmer, Inc), and their geometries have been optimized with ChemBio 3D Ultra 13.0 (PerkinElmer, Inc) using MM2 force field until a minimum 0.100 root-mean-square gradient was reached. Subsequently, all compound structures were followed by energy minimization with MMFF94x force field in the molecular operating environment (MOE) Software package 2014.0901. Conformational search for ligand preparation was carried out by the MOE LowModelMD method, which performs molecular dynamic perturbations along with low-frequency vibrational modes with energy window of 7 kcal/mol, and conformational limits of 1000.

Receptor preparation The X-ray crystallographic structure of a complex of DNase I and the self-complementary octamer duplex $d(GGTATACC)_2$ (PDB code: 1DNK) was obtained from the Protein Data Bank.[42] The errors of DNase I were corrected by the structure preparation process in MOE. After the correction, hydrogens were added and partial charges (Gasteiger methodology) were calculated. Energy minimization (AMBER12:EHT, root mean square gradient: 0.100) was performed.

Binding site selection The Site Finder module of the MOE was used to identify possible ligand-binding pockets within the optimized structure of DNase I. Hydrophobic or hydrophilic alpha spheres served as probes denoting zones of tight atom packing. These alpha spheres were used to define and rank potential ligand-binding sites according to their propensity for ligand

binding score, which was based on the amino acid composition of the pocket.[43]

Docking protocol The molecular docking study was performed using MOE to understand the ligand-protein interactions in detail. The default Triangle Matcher placement method was used for the induced fit docking. The generalized born volume integral/weighted surface area (GBVI/WSA) dG scoring function, which estimates the free energy of binding of the ligand from a given pose, was used to rank the final poses. Each ligand-protein complex with the lowest relative binding free energy (ΔG) score was selected. A more negative score indicates that the ligand is more likely to dock with the receptor and achieve more favorable interactions.

Molecular dynamics simulation
The molecular dynamics simulation of the DNase I-compound **9** docking complex was carried out using Desmond, implemented in Schrödinger 2015-1 software. Forcefield parameters for the protein-ligand system were assigned using the AMBER12:EHT forcefield. The structure of the added water was based on the simple point charge (SPC) solvent model. The system was neutralized with Na^+ ions to balance the net charge of the whole simulation box to neutral. The final system contained approximately 29 120 atoms. The system was passed through a 6-step relaxation protocol before molecular dynamics simulations. The relaxed system was simulated for 10 ns, using an normal pressure temperature (NPT) ensemble with a Nosé-Hoover thermostat at 310 K and Martyna-Tobias-Klein barostat at 1.01325 bar pressure. Atomic coordinate data and system energies were recorded every 1 ps. The root mean square deviation (RMSD) and root mean square fluctuation (RMSF) of the protein-ligand complex were analyzed with respect to simulation time.

Protein structure alignment
The superposition of human DNase I (PDB: 4AWN) with the bovine pancreatic DNase I (PDB: 1DNK) was performed using the Protein structure alignment feature in Maestro.[38] Using the default matrix embedded in the program, the calculation was run until the maximum number of aligned atoms with the lowest RMSD was obtained. An alignment score lower than 0.6-0.7 indicated a good alignment.[44] The number of identical amino acid residues in examined DNases I was compared with the percentage of sequence similarity and was displayed by the color matching residues scheme.

3 | RESULTS AND DISCUSSION

3.1 | DNase I inhibition

Four of the 19 studied benzimidazoles inhibited bovine pancreatic DNase I with an IC_{50} value below 200 μM (Table 2), whereby 1 compound (**1**) belonged to 1,3-disubstituted-benzimidazole-2-imines, 1 (**9**) belonged to 2-substituted-1, 3-thiazolo[3,2-*a*]benzimidazolones, and 2 compounds (**14** and **19**) belonged to 1,3-disubstituted-benzimidazole-2-thiones. Compound **9** was shown to be the most potent DNase I inhibitor with an IC_{50} value of 79.46 ± 11.75 μM. Crystal violet, used as positive control, exhibited weaker DNase I inhibition ($IC_{50} = 351.82 \pm 29.41$ μM) compared with compounds **1**, **9**, **14**, and **19**. Due to the lack of organic DNase I inhibitors, compound **9** could be set as a novel standard DNase I inhibitor used in further investigations.

3.2 | R-group analysis

As the Pharma RQSAR model showed, the presence of hydrogen-bond acceptor substituents at R2, R3, and R4

TABLE 2 DNase I inhibition by benzimidazoles **1-19**

Compound	DNase I inhibition IC_{50} (μM) ± SD	Compound	DNase I inhibition IC_{50} (μM) ± SD
1	151.19 ± 14.80	**11**	>200
2	>200	**12**	>200
3	>200	**13**	>200
4	>200	**14**	89.85 ± 17.20
5	>200	**15**	>200
6	>200	**16**	>200
7	>200	**17**	>200
8	>200	**18**	>200
9	79.46 ± 11.75	**19**	96.38 ± 19.27
10	>200	Crystal violet	351.82 ± 29.41

Note. SD, standard deviation.

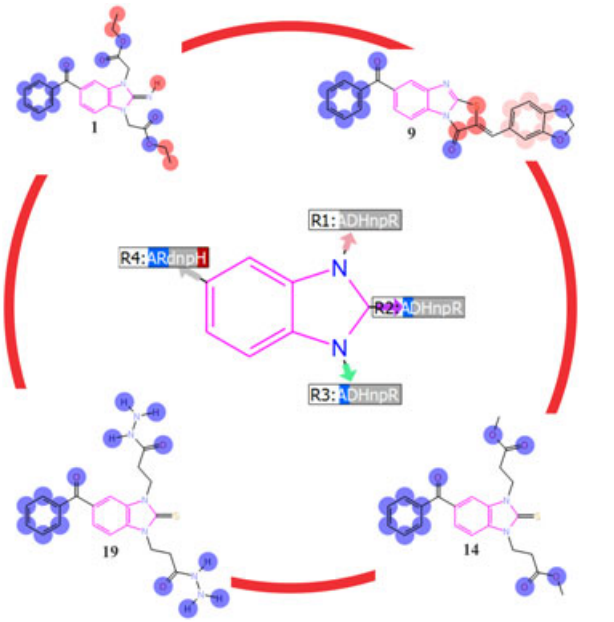

FIGURE 1 The Pharma RQSAR model of the studied benzimidazoles. The attachment positions on the benzimidazole ring were labeled with a list of pharmacophore features, colored by significance: blue for significant positive contributions, red for significant negative contributions, and gray for insignificant contributions to DNase I inhibition. If a pharmacophore feature was absent from an attachment position, a lower-case letter was used for the pharmacophore feature type. Examined pharmacophore features: hydrogen-bond acceptor (A), hydrogen-bond donor (D), hydrophobic (H), negatively charged (N), positively charged (P), and aromatic (R). DNase I, deoxyribonuclease I; RQSAR, R-group quantitative structure-activity relationship

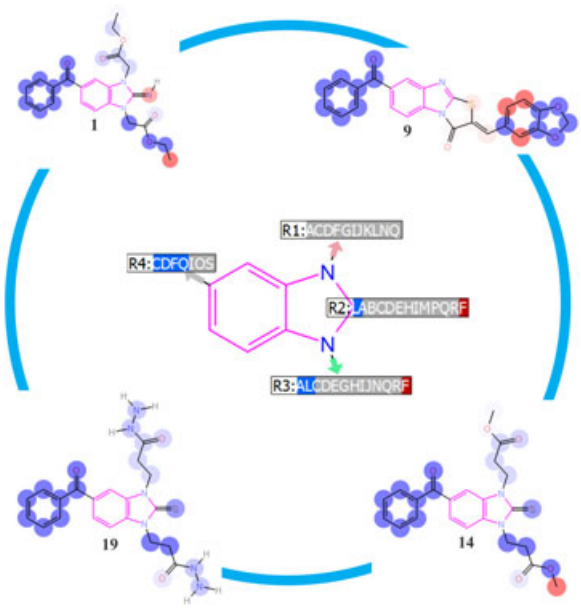

FIGURE 2 The E-State RQSAR model of the studied benzimidazoles. The attachment positions on the benzimidazole ring were labeled with a list of letters representing the E-state atom types (Supporting Information Table S2), colored by significance: blue for significant positive contributions, red for significant negative contributions, and gray for insignificant contributions to DNase I inhibition. If an E-state atom type was absent from an attachment position, it was not included in the annotation for that position. DNase I, deoxyribonuclease I; RQSAR, R-group quantitative structure-activity relationship

positions, as well as the presence of aryl substituents at R4 position of the studied benzimidazoles, substantially increased DNase I inhibition. However, the presence of hydrophobic substituents at R4 position resulted in a decreased DNase I inhibition (Supporting Information Table S1, Figure 1). Next, we examined the effect of the E-State parameters of benzimidazoles on DNase I inhibition (Supporting Information Table S2, Figure 2). As shown in Supporting Information Table S2, the introduction of aasC, dssC, aaCH, and dO fragments at R4 position, $ssCH_2$ and ssO fragments at R3 position, as well as the introduction of ssO fragment at R2 position exerted a significant enhancement to the benzimidazoles activity. On the contrary, the use of aaCH fragment at R2 and R3 positions resulted in a decreased DNase I inhibition (Supporting Information Table S2, Figure 2). In addition, we wanted to examine how sensitive the DNase I inhibitory property of benzimidazoles was to R group variation at specific position. As shown in Figure 3, variations of substituents at R2, R3, and R4 positions had substantial effects on DNase I inhibition compared with the benzimidazole scaffold or substituents at R1 position.

3.3 | 3D pharmacophore modeling

The best hypothesis model for the studied benzimidazoles was selected by analyzing the survival scores in Supporting Information Table S3. Of note, the model with the best survival score can differentiate between the actives and inactives.[41] The selected common pharmacophore hypothesis had 5 features namely, 2 acceptor groups (A) and 3 aromatic groups (R). The result is presented in Figure 4, which depicts the superimposed images of the active benzimidazoles with the generated hypothesis. The angle and distances between different sites of the model are given in Supporting Information Tables S4 and S5, respectively. The AARRR.243 hypothesis highlighted the 3D space arrangement among

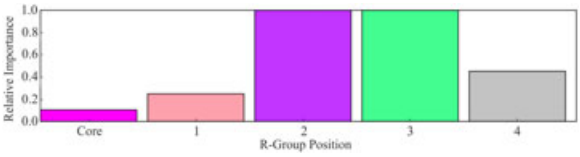

FIGURE 3 The Importance analysis histogram of the studied benzimidazoles

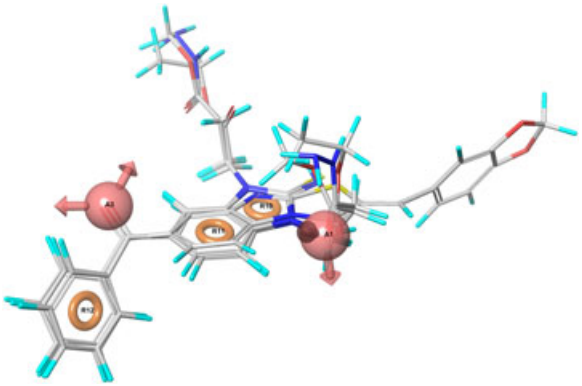

FIGURE 4 Superimposed images of the active benzimidazoles with AARRR.243 hypothesis

hydrogen-bond substituents and aromatic rings at benzimidazoles (Figure 4) and confirmed the results of the Pharma RQSAR model at R3 and R4 positions (Supporting Information Table S1).

3.4 | Molecular docking

The binding site residues in DNase I have been identified using the Site Finder module implemented in the MOE software. The results from the analysis highlighted that amino acid residues like Asn 7, Arg 9, Glu 39, Tyr 76, Glu 78, Arg 111, His 134, Ala 136, Pro 137, Asp 168, Asn 170, Thr 203, Thr 205, Thr 207, Tyr 211, Asp 251, and His 252 constituted the binding pocket of DNase I structure (Supporting Information Table S6). Our results are consistent with a recent study highlighting the conservation of the amino acids involved in the identified cation-binding sites across DNase I and DNase I-like protein.[39] It is worth mentioning that inhibitor-binding pocket, represented by a gray-red surface map, is within the region that interacts with DNA octamer d(GGTATACC)$_2$ (Figure 5).

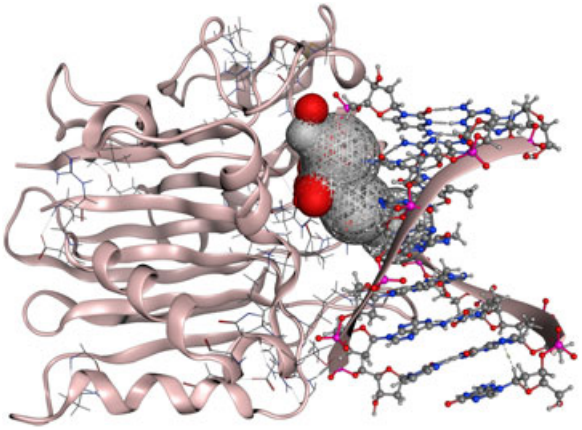

FIGURE 5 The top-ranked DNase I binding site. DNase I, deoxyribonuclease I

The intermolecular contacts between benzimidazoles and DNase I was analyzed using the ligand interaction diagram of MOE suite. It illustrates the existence of hydrogen bond, pi-cation, and H-pi interactions (Supporting Information Table S7). In addition, the bond distances and bond energy between the inhibitor and receptor atoms were also examined. Of note, the importance of Glu 39, His 134, and His 252 residues in the catalytic mechanism of DNase I has been already highlighted.[39] It was confirmed that catalytic residues His 134 and His 252 are a part of the ion binding site IV, which is implicated in the cleavage of scissile phosphate. Furthermore, several site-directed mutagenesis experiments on the residues surrounding His 134 and His 252 demonstrated that single mutations on a Glu 39 residue resulted in a very low activities on a DNA molecule.[45,46] The effects of these mutations also confirmed the active role of Glu 39 in the IV catalytic site.

The interaction profiles of benzimidazoles with DNase I domain are shown in Figure 6 and Supporting Information Table S7. In addition, the positive correlation between the IC_{50} inhibition values and the relative binding free energies of the most active benzimidazoles are shown in Table 2 and Supporting Information Table S7. The physicochemical descriptors of active molecules are shown in Supporting Information Table S8. Compound **9**, which corresponds to one of the most promising ligands reported in this series, showed a dominant hydrogen bond interaction with His 134 catalytic residue (Figure 6D). Furthermore, identical interaction was also observed for the second most active compound **14** (Figure 6F). In addition, these compounds exhibited some minor H-pi, pi-cation, and H-donor interactions with Tyr 211, Arg 111, and Asp 251 residues (Supporting Information Table S7). The results from Supporting Information Table S7 indicate that benzimidazoles **1** and **19** were not found to possess any similar interaction as previously discussed compounds. These compounds were observed to interact with other conserved catalytic residues such as Glu 39 or His 252. It was shown that compound **1** forms hydrogen bond interactions with both catalytic residues (Figure 6A). Furthermore, compound **19** was exhibiting hydrogen bond interactions with residues such as Tyr 76, Ser 110, Arg 111, Ala 136, and Pro 137 along with the catalytic Glu 39 residue (Figure 6H). Consequently, the presence of interactions with the most important catalytic residues of DNase I binding pocket are expected to enhance the efficiency of benzimidazoles.

3.5 | Molecular dynamics simulation

The study was further extended to assess the stability of DNase I-compound **9** docking complex through molecular

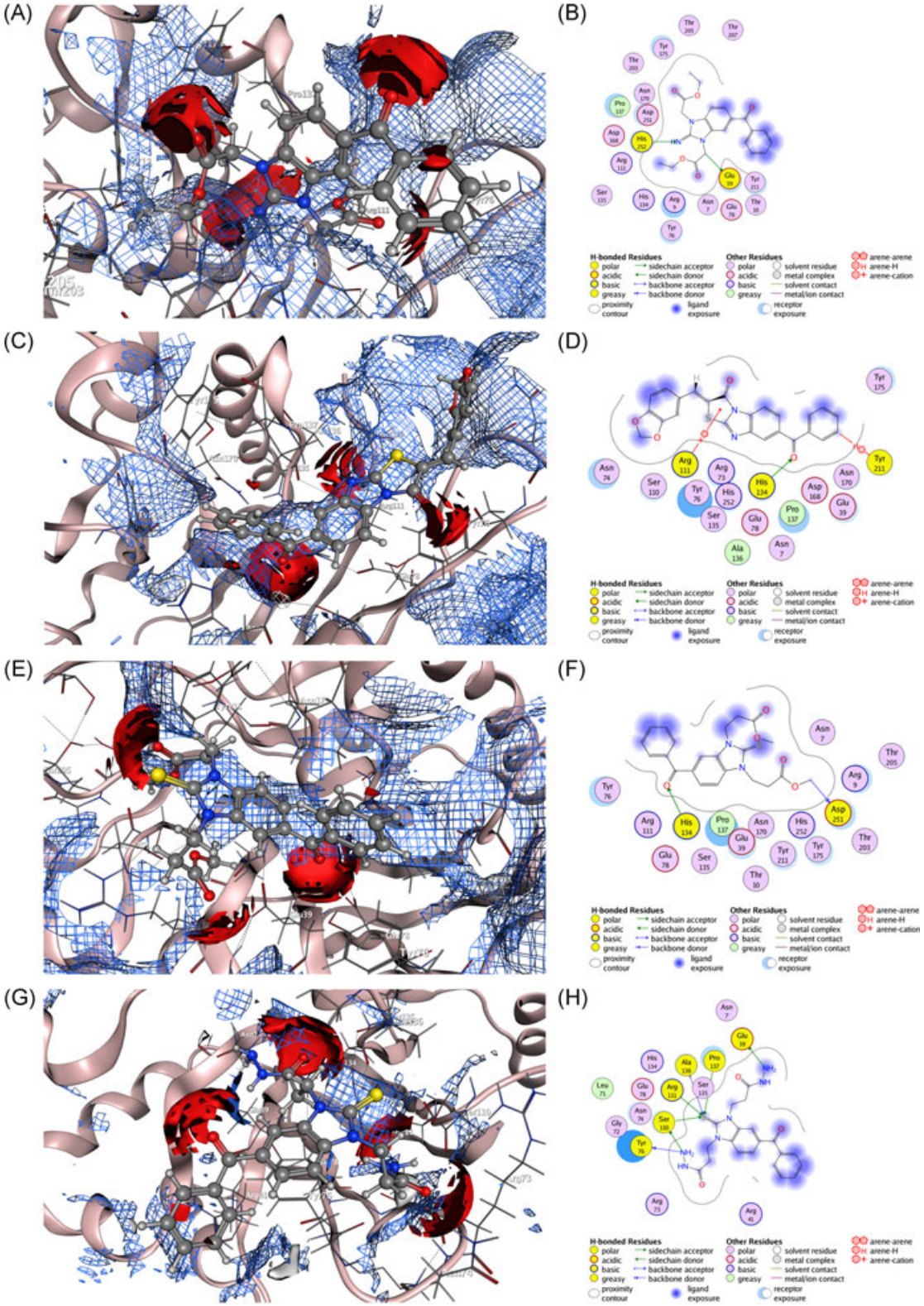

FIGURE 6 Binding interaction of the benzimidazoles with DNase I (PDB: 1DNK) domain: (A,B) 3D/2D binding pose of the compound **1**; (C,D) 3D/2D binding mode of the most active compound **9**; (E,F) 3D/2D binding mode of the second most active compound **14**; and (G,H) 3D/2D binding mode of compound **19**. DNase I, deoxyribonuclease I

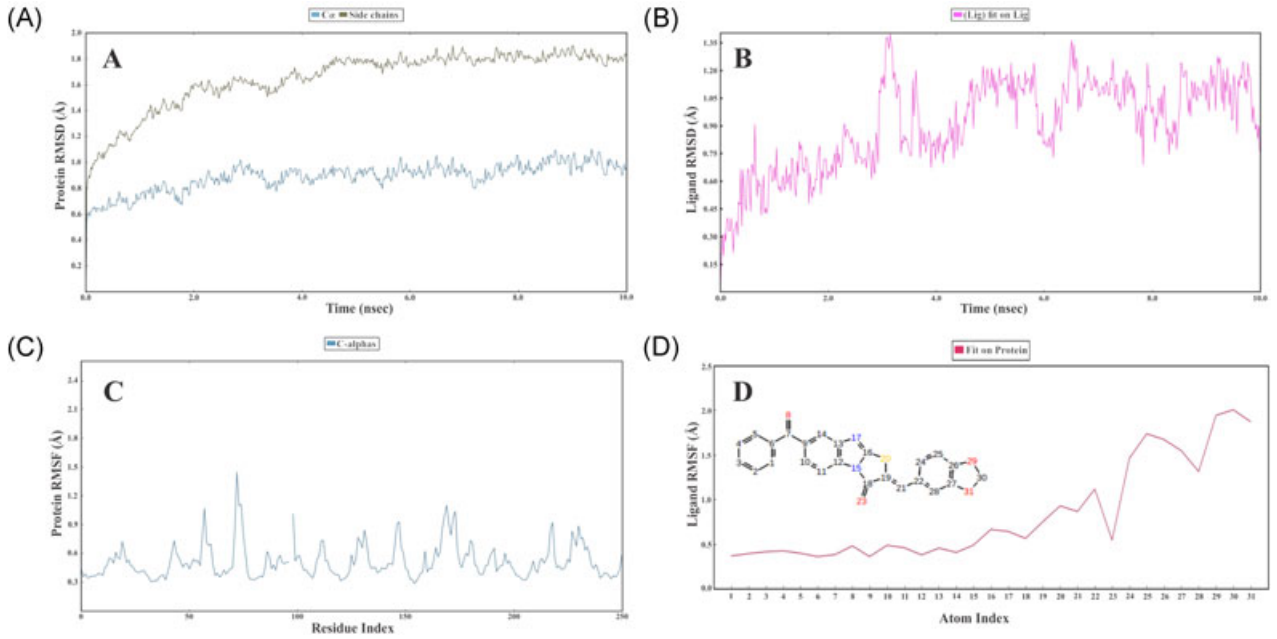

FIGURE 7 (A,B) RMSD plot of bovine pancreatic DNase I and compound **9** during the course of 10 ns molecular dynamics simulation; (C,D) RMSF plot of bovine pancreatic DNase I and compound **9** during the simulation trajectory. DNase I, deoxyribonuclease I; RMSD, root mean square deviation

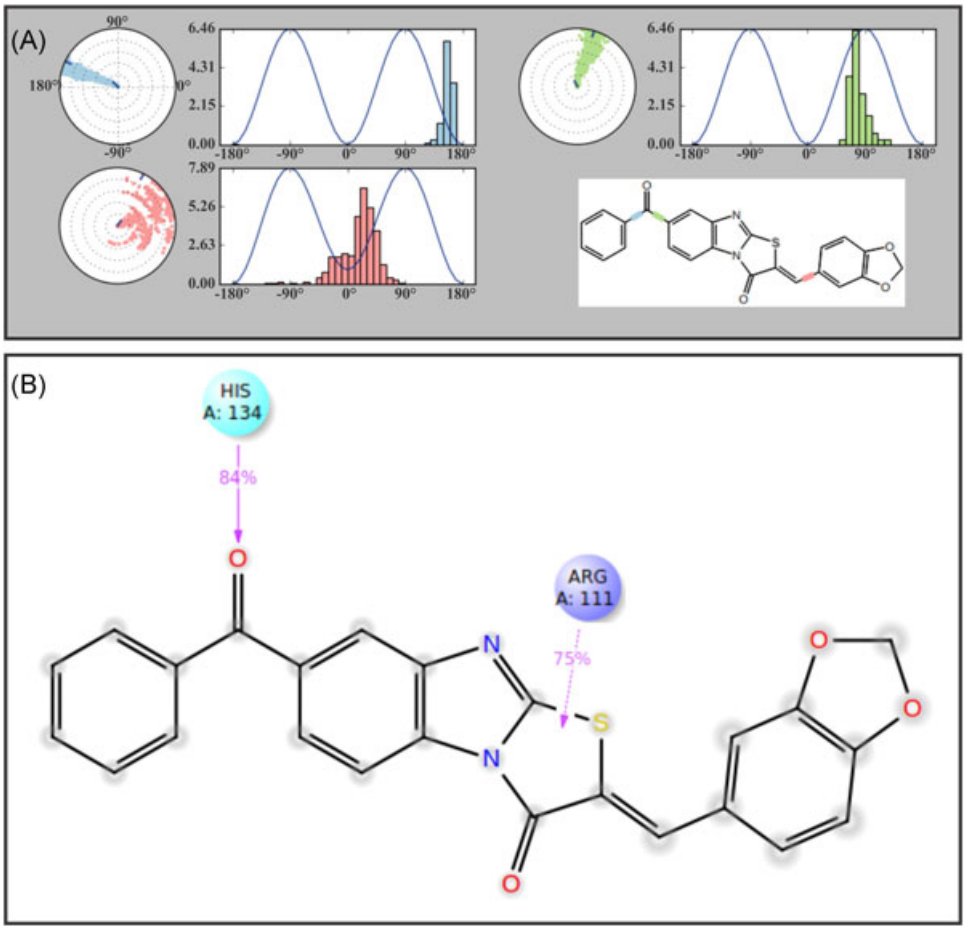

FIGURE 8 (A) The ligand torsions plot summarizes the conformational evolution of every rotatable bond in compound **9** throughout the course of 10 ns molecular dynamics simulation; (B) Interactions of bovine pancreatic DNase I and compound **9** during the simulation trajectory. DNase I, deoxyribonuclease I

dynamics simulation (Supporting Information animation content S1). The RMSD and RMSF plots for DNase I and compound **9** (Figure 7) showed that docking complex was stable during entire simulation period. The RMSD for Cα, side chains and heavy atoms remained within the limit of 2 Å (Figure 7A,B). The similar situation was noted for RMSF values (Figure 7C,D). The obtained results indicated small structural rearrangement, less conformational changes and confirmed DNase I complex stability.[38] Once the conformational stability of the system was established, interaction stability of the system was monitored. The interactions observed during 10 ns molecular simulation showed hydrogen bond interaction with catalytic His 134 and pi-cation interaction with Arg 111 (Figure 8). The importance of carbonyl group in docking position of compound **9** (Figure 6, Supporting Information Table S7) was further confirmed by conformational strain that ligand undergoes to maintain a protein-bound conformation (Figure 8A). Furthermore, it was shown that 84% of the simulation time, compound **9** interacts with catalytic His 134 (Figure 8B).

3.6 | Protein structure alignment

Sequence alignments of DNA-interacting residues of DNase I from different species are in detail explained by Pan et al.[46] The authors showed that human DNase I shares 78% sequence similarity with the bovine enzyme. Of all the residues that directly contact DNA in either bovine DNase I-octamer complex,[42] only 2 are different in the human enzyme.[47] At positions 9 and 206, human DNase I has Gln and Pro, respectively, whereas Arg and Ser are found in bovine DNase I. These observations are similar with our results shown in Supporting Information Figure S1. The superposition of human DNase I[48] with bovine pancreatic DNase I[42] showed that human DNase I shares 89% sequence similarity with bovine DNase I (Supporting Information Figure S1). Our improved sequence similarity results could be explained by the more resolved X-ray crystal structure of human DNase I at 1.95 Å.[48] Furthermore, the protein structure alignment showed that binding site residues identified by the Site Finder module are identical for bovine and human DNase I (Supporting Information Figure S1). These results suggest the potential translational impact of benzimidazoles against human DNase I.

4 | CONCLUSION

In summary, 4 of 19 investigated benzimidazoles (compounds **1**, **9**, **14**, and **19**) inhibited bovine pancreatic DNase I with IC_{50} values below 200 μM, with compound **9** being the most potent ($IC_{50} = 79.46 \pm 11.75$ μM). These 4 compounds showed higher DNase I inhibitory activity then crystal violet ($IC_{50} = 351.82 \pm 29.41$ μM), used as positive control. The in silico methods showed a significant enhancement of benzimidazoles activity using hydrogen-bond acceptor substituents at R2, R3, and R4 positions, or aryl substituents at R4 position. Furthermore, the benzimidazoles interactions with the most important catalytic residues of DNase I, including H-acceptor interaction with residue His 134 and His 252 and/or H-donor interaction with residue Glu 39, were shown. In addition, a molecular dynamics simulation was performed for DNase I-compound **9** docking complex. Trajectory analysis showed that docking complex and intermolecular interactions were stable throughout the entire production part of simulations. The results of the protein structure alignment module suggested the potential translational impact of benzimidazoles against human DNase I. Benzimidazoles can be regarded as a promising scaffold for design of new DNase I inhibitors and could have potential therapeutic applications due to the significant involvement of DNase I in pathophysiology of many disease conditions. To the best of our knowledge, this is the first report on DNase I inhibition by benzimidazoles.

ACKNOWLEDGMENTS

The financial support to this work by Ministry of Education, Science and Technological Development of the Republic of Serbia (Grants no. OI 172044, OI 171025, and TR 31060), and Faculty of Medicine of the University of Nis (Internal project No. 4) is gratefully acknowledged. The authors would like to thank Chemical Computing Group and Schrödinger LLC for providing us the academic licenses free of cost for this study.

CONFLICTS OF INTEREST

The authors declare that there are no conflicts of interest.

ORCID

Andrija Šmelcerović http://orcid.org/0000-0001-7724-0967

REFERENCES

1. Thompson C. Apoptosis in the pathogenesis and treatment of disease. *Science*. 1995;267:1456-1462.
2. Elmore S. Apoptosis: a review of programmed cell death. *Toxicol Pathol*. 2007;35:495-516.

3. Heintz N. Cell death and the cell cycle: a relationship between transformation and neurodegeneration? *Trends Biochem Sci*. 1993;18:157-159.
4. Isacson O. On neuronal health. *Trends Neurosci*. 1993;16: 306-308.
5. Oliveri M, Daga A, Cantoni C, Lunardi C, Millo R, Puccetti A. DNase I mediates internucleosomal DNA degradation in human cells undergoing drug-induced apoptosis. *Eur J Immunol*. 2001;31:743-751.
6. Rosenbaum DM, Kalberg J, Kessler JA. Superoxide dismutase ameliorates neuronal death from hypoxia in culture. *Stroke*. 1994;25:857-862.
7. Tanaka M, Ito H, Adachi S, et al. Hypoxia induces apoptosis with enhanced expression of Fas antigen messenger RNA in cultured neonatal rat cardiomyocytes. *Circ Res*. 1994;75: 426-433.
8. Goldin RD, Hunt NC, Clark J, Wickramasinghe SN. Apoptotic bodies in a murine model of alcoholic liver disease: reversibility of ethanol-induced changes. *J Pathol*. 1993;171:73-76.
9. Oliveri M, Daga A, Lunardi C, Navone R, Millo R, Puccetti A. DNase I behaves as a transcription factor which modulates Fas expression in human cells. *Eur J Immunol*. 2004;34: 273-279.
10. Peitsch MC, Polzar B, Stephan H, et al. Characterization of the endogenous deoxyribonuclease involved in nuclear DNA degradation during apoptosis (programmed cell death). *EMBO J*. 1993;12:371-377.
11. Polzar B, Peitsch MC, Loos R, Tschopp J, Mannherz HG. Overexpression of deoxyribonuclease I (DNase I) transfected into COS-cells: its distribution during apoptotic cell death. *Eur J Cell Biol*. 1993;62:397-405.
12. Rauch F, Polzar B, Stephan H, Zanotti S, Paddenberg R, Mannherz HG. Androgen ablation leads to an upregulation and intranuclear accumulation of deoxyribonuclease I in rat prostate epithelial cells paralleling their apoptotic elimination. *J Cell Biol*. 1997;137:909-923.
13. Samejima K, Earnshaw WC. Trashing the genome: the role of nucleases during apoptosis. *Nat Rev Mol Cell Biol*. 2005;6: 677-688.
14. Yao M, Keogh A, Spratt P, dos Remedios CG, Kießling PC. Elevated DNase I levels in human idiopathic dilated cardiomyopathy: an indicator of apoptosis? *J Mol Cell Cardiol*. 1996;28:95-101.
15. Zhu B, Gong Y, Chen P, Zhang H, Zhao T, Li P. Increased DNase I activity in diabetes might be associated with injury of pancreas. *Mol Cell Biochem*. 2014;393:23-32.
16. Zhu B, Zhang L, Zhang YY, et al. DNase I aggravates islet β-cell apoptosis in type 2 diabetes. *Mol Med Rep*. 2016;13:4577-4584.
17. Takeda M, Fukuoka K, Endou H. Cisplatin-induced apoptosis in mouse proximal tubular cell line. In: Koide H, Ichikawa I, eds. *Progression of Chronic Renal Diseases. Contributions to Nephrology*. Vol. 118. Basel: Karger; 1996:pp. 24-28.
18. Yin X, Apostolov EO, Shah SV, et al. Induction of renal endonuclease G by cisplatin is reduced in DNase I-deficient mice. *J Am Soc Nephrol*. 2007;18:2544-2553.
19. Basnakian AG, Apostolov EO, Yin X, Napirei M, Mannherz HG, Shah SV. Cisplatin nephrotoxicity is mediated by deoxyribonuclease I. *J Am Soc Nephrol*. 2005;16:697-702.
20. Napirei M, Basnakian AG, Apostolov EO, Mannherz HG. Deoxyribonuclease 1 aggravates acetaminophen-induced liver necrosis in male CD-1 mice. *Hepatology*. 2006;43: 297-305.
21. Apostolov EO, Soultanova I, Savenka A, et al. Deoxyribonuclease I is essential for DNA fragmentation induced by gamma radiation in mice. *Radiat Res*. 2009;172:481-492.
22. Kolarevic A, Yancheva D, Kocic G, Smelcerovic A. Deoxyribonuclease inhibitors. *Eur J Med Chem*. 2014;88:101-111.
23. Liao TH, McKenzie LJ. Inactivation of bovine pancreatic DNase by 2-nitro-5-thiocyanobenzoic acid. I. A novel inhibitor for DNase I. *J Biol Chem*. 1979;254:9598-9601.
24. Chen WJ, Liao TH. 2-Nitro-5-thiosulfobenzoic acid as a novel inhibitor specific for deoxyribonuclease I. *Protein J*. 2008;27: 240-246.
25. Doctor VM. Inhibition of deoxyribonuclease I of human serum in vitro by nitrogen mustard or leucocyte extracts. *Arch Biochem Biophys*. 1962;96:475-478.
26. Zhou Z, Zhu C, Ren J, Dong S. A graphene-based real-time fluorescent assay of deoxyribonuclease I activity and inhibition. *Anal Chim Acta*. 2012;740:88-92.
27. Narasimhan B, Sharma D, Kumar P. Benzimidazole: a medicinally important heterocyclic moiety. *Med Chem Res*. 2012;21:269-283.
28. Salahuddin, Shaharyar M, Mazumder A. Benzimidazoles: a biologically active compounds. *Arab J Chem*. 2017;10: S157-S173.
29. Bansal Y, Silakari O. The therapeutic journey of benzimidazoles: a review. *Bioorg Med Chem*. 2012;20:6208-6236.
30. Akhtar J, Khan AA, Ali Z, Haider R, Shahar Yar M. Structure-activity relationship (SAR) study and design strategies of nitrogen-containing heterocyclic moieties for their anticancer activities. *Eur J Med Chem*. 2017;125:143-189.
31. Mavrova AT, Anichina KK, Vuchev DI, et al. Antihelminthic activity of some newly synthesized 5(6)-(un)substituted-1*H*-benzimidazol-2-ylthioacetylpiperazine derivatives. *Eur J Med Chem*. 2006;41:1412-1420.
32. Mavrova AT, Anichina KK, Vuchev DI, Tsenov JA, Kondeva MS, Micheva MK. Synthesis and antitrichinellosis activity of some 2-substituted-[1,3]thiazolo[3,2-*a*]benzimidazol-3(2*H*)-ones. *Bioorg Med Chem*. 2005;13:5550-5559.
33. Mavrova AT, Vuchev D, Anichina K, Vassilev N. Synthesis, antitrichinnellosis and antiprotozoal activity of some novel thieno[2,3-*d*]pyrimidin-4(3*H*)-ones containing benzimidazole ring. *Eur J Med Chem*. 2010;45:5856-5861.
34. Mavrova AT, Wesselinova D, Vassilev N, Tsenov JA. Design, synthesis and antiproliferative properties of some new 5-substituted-2-iminobenzimidazole derivatives. *Eur J Med Chem*. 2013;63:696-701.
35. Mavrova AT, Wesselinova D, Vassilev N, Tsenov JA. Synthesis, characterization and cytotoxicity of some novel 1,3-disubstituted-2,3-dihydro-2-iminobenzimidazoles. *Eur J Med Chem*. 2011;46:3362-3367.
36. Mavrova AT, Yancheva D, Anastassova N, et al. Synthesis, electronic properties, antioxidant and antibacterial activity of some new benzimidazoles. *Bioorg Med Chem*. 2015;23:6317-6326.
37. Anastassova NO, Mavrova AT, Yancheva DY, et al. Hepatotoxicity and antioxidant activity of some new N, N′-disubstituted benzimidazole-2-thiones, radical scavenging mechanism and structure-activity relationship. *Arab J Chem*. 2018;11:353-369.

38. Small-Molecule Drug Discovery Suite 2015-1. LLC, New York, NY: Schrödinger; 2015.
39. Guéroult M, Picot D, Abi-Ghanem J, Hartmann B, Baaden M. How cations can assist DNase I in DNA binding and hydrolysis. *PLoS Comput Biol*. 2010;6:e1001000.
40. Bartholeyns J, Peeters-Joris C, Reychler H, Baudhuin P. Hepatic nucleases. 1. Methods for the specific determination and characterization in rat liver. *Eur J Biochem*. 1975;57:205-211.
41. Dixon SL, Smondyrev AM, Knoll EH, Rao SN, Shaw DE, Friesner RA. PHASE: a new engine for pharmacophore perception, 3D QSAR model development, and 3D database screening: 1. Methodology and preliminary results. *J Comput Aided Mol Des*. 2006;20:647-671.
42. Weston SA, Lahm A, Suck D. X-ray structure of the DNase I-d $(GGTATACC)_2$ complex at 2.3 Å resolution. *J Mol Biol*. 1992;226:1237-1256.
43. Soga S, Shirai H, Kobori M, Hirayama N. Use of amino acid composition to predict ligand-binding sites. *J Chem Inf Model*. 2007;47:400-406.
44. Yang AS, Honig B. An integrated approach to the analysis and modeling of protein sequences and structures. I. Protein structural alignment and a quantitative measure for protein structural distance. *J Mol Biol*. 2000;301:665-678.
45. Jones SJ, Worrall AF, Connolly BA. Site-directed mutagenesis of the catalytic residues of bovine pancreatic deoxyribonuclease I. *J Mol Biol*. 1996;264:1154-1163.
46. Pan CQ, Ulmer JS, Herzka A, Lazarus RA. Mutational analysis of human DNase I at the DNA binding interface: Implications for DNA recognition, catalysis, and metal ion dependence. *Protein Sci*. 1998;7:628-636.
47. Wolf E, Frenz J, Suck D. Structure of human pancreatic DNase I at 2.2 Å resolution. *Protein Eng*. 1995;8(Suppl):79.
48. Parsiegla G, Noguere C, Santell L, Lazarus RA, Bourne Y. The structure of human DNase I bound to magnesium and phosphate ions points to a catalytic mechanism common to members of the DNase I-like superfamily. *Biochemistry*. 2012;51:10250-10258.

SUPPORTING INFORMATION

Additional supporting information may be found online in the Supporting Information section at the end of the article.

How to cite this article: Kolarević A, Ilić BS, Anastassova N, et al. Benzimidazoles as novel deoxyribonuclease I inhibitors. *J Cell Biochem*. 2018;1-12. https://doi.org/10.1002/jcb.27147